Indonesian Journal of Science & Technology

Journal homepage: http://ejournal.upi.edu/index.php/ijost/

Synthesis, Characterization, and Electrochemical Performance of Reduced Graphene Oxide-Metal (Cu,Zn)-Oxide Materials

Sugianto Sugianto[1,], Ngurah Made Dharma Putra[1], Endah F. Rahayu[2], Wahyu B. Widayatno[3], Cherly Firdharini[3], Slamet Priyono[3], Didik Aryanto[3]*

[1]Department of Physics, Universitas Negeri Semarang, Indonesia
[2]Department of Chemistry, Universitas Negeri Semarang, Indonesia
[3]Research Center for Advance Materials, Badan Riset dan Inovasi Nasional, Indonesia
*Correspondence: E-mail: sugianto@mail.unnes.ac.id

ABSTRACT

The reduced graphene oxide (rGO) and metal (Cu,Zn)-oxide composites were prepared using a one-step hydrothermal technique. The role of (Cu,Zn)-oxide on the physical and electrochemical properties of the composite was investigated. The composite consists of various shapes of ZnO nanoflowers and micro-spheres, as well as Cu-oxide nanoflakes and octahedron-like shapes. The (Cu,Zn)-oxides were formed in between the rGO layers and observed in the rGO-ZnO, rGO-CuO, and rGO-CuO-ZnO composites. The presence of ZnO, CuO, and rGO within the composite structure is also confirmed by the analyses of crystal structure, microstructure, and surface functional groups. Some excess impurities remaining from the surfactant give considerable differences in the electrochemical performance of the composites. The specific capacitance values of the rGO, rGO-ZnO, rGO-CuO, rGO-(0.5CuO-0.5ZnO), and rGO-(0.25CuO-0.75ZnO) composites are 9.32, 58.53, 54.14, 25.21, and 69.27 F/g, respectively. The formation of a double metal-oxide structure as well as their insertion into the rGO sheet can significantly improve the electrochemical properties of the supercapacitor.

ARTICLE INFO

Article History:
Submitted/Received 13 Jan 2023
First Revised 26 Feb 2023
Accepted 07 Mar 2023
First Available online 08 Mar 2023
Publication Date 01 Sep 2023

Keyword:
Composite,
Cu-oxide,
Morphology,
Reduced graphene oxide (rGO),
Zinc oxide (ZnO).

1. INTRODUCTION

Supercapacitors have attracted tremendous attention and one of the most considerable scientific interests in recent years. This is because of their potential as one of the candidates for advanced materials in energy storage device applications. They can store and discharge a large quantity of energy very quick (Otun *et al.*, 2022). However, there is an issue relating to the energy density, which is lower than that of Li-ions batteries (Otun *et al.*, 2022). To improve the energy density, some researchers tried to incorporate the electrical double-layer capacitor (EDLC) and pseudocapacitive capacitor (Rai *et al.*, 2021), where their performance has a direct correlation to the dependence on the quality of the electrode materials. EDLC uses carbon-based materials as an electrode because of their excellent properties such as highly porous structure, good adsorption properties, large surface area, high electrical conductivity (Faraji & Ani, 2015), transition metal nitrides (Dong *et al.*, 2013), various transition oxides (Xie *et al.*, 2013; Selvekumar *et al.*, 2012, Aravinda *et al.*, 2013), and conducting polymers (Firoz *et al.*, 2013; Ghenaatian *et al.*, 2012). This material is also utilized as electrodes in the pseudocapacitor owing to its high theoretical capacitance (Zhou & Ma, 2015). Herein, the oxygen surface functional groups may facilitate a faradic reaction that can enhance the capacitance and self-discharge features. In addition, the existence of transition metal oxide within the carbon-based EDLC electrodes has a direct impact on the improvement of specific capacitance than that of pristine carbon (Miah *et al.*, 2020).

In previous studies, various transition metal oxides (e.g. ruthenium oxide (RuO_2), nickel oxide (NiO), cobalt oxide (Co_2O_3), manganese oxide (MnO_2), copper oxide (CuO), zinc oxide (ZnO), etc) have been incorporated along with carbon-based materials as a prospective electrode for supercapacitor applications (Majeed *et al.*, 2015). The results implied that the electrochemical performance can be enhanced to some extent by the presence of metal oxide. Graphene and graphene oxide (GO) have been also frequently used in supercapacitors. This is because of their high specific area and electrical conductivity (Maity *et al.*, 2018). Recently, reduced graphene oxide (rGO) is also used as a prospective material for altering graphene. Graphene possesses strong π-π interaction which leads to the accumulation of graphene oxide sheets, and further to the reduction of a specific area, giving limitations to the usage of graphene in supercapacitors (Ray *et al.*, 2021). From the combination of the specific characteristics of metal oxide and rGO, the composite of metal-oxide/rGO has been prepared using the chemical method. Here, to the best of our knowledge, only a few studies reported the combination of metal oxide and rGO for supercapacitor applications. ZnO with a 3.2 eV bandgap is likely the most promising electrode material because of its low cost, high energy density (650 Ah/g), high chemical stability, and good electrochemical activity (Otun *et al.*, 2022; Alver *et al.*, 2016). Similarly, CuO with a 1.2 eV bandgap also possesses some positive features, including good electrical conductivity, high specific surface area, manageable surface morphology, and enhanced electrochemical efficiency (Lohar *et al.*, 2021). Besides, CuO is inexpensive, non-toxic, chemically/thermally stable, and possesses high theoretical capacitance (~1800 F/g) (Wu *et al.*, 2017). Previous studies revealed that the ZnO-rGO (Prabhuraj *et al.*, 2021; Miah *et al.*, 2020, Rai *et al.*, 2021), CuO-rGO (Sagadevan *et al.*, 2018; Lohar *et al.*, 2021), CuO-ZnO (Wu *et al.*, 2017), and N-rGO-CuO-ZnO (Maity *et al.*, 2018) demonstrated good super capacitive properties. This is because of its good charge-discharge, high specific capacitance, and long cycling life.

Based on the previous reports, ZnO-rGO, CuO-rGO, and ZnO-CuO-rGO composites can

DOI: https://doi.org/10.17509/ijost.v8i2.56065
p- ISSN 2528-1410 e- ISSN 2527-8045

be synthesized using several methods. Miah *et al*. (2020) and Du *et al*. (2019) prepared each composite part separately before final mixing. Alternatively, the forming process of ZnO or CuO can be carried out in GO suspension using coprecipitation or solvothermal methods (Rai *et al*., 2021; Kumar *et al*., 2020; Praburaj *et al*., 2021; Sagadevan *et al*., 2018), where strong solutions such as H_2SO_4, ammonia, etc are used. Maity *et al*. (2018) reported the synthesis route that is simple, facile, the cheapest, and eco-friendly route for producing ZnO or CuO -rGO composite, but they still used ammonia during the composite synthesis. It is reported that ZnO or CuO has a single shape, like a sphere, flake, or rod. Until now, no one has reported the multi-shape behavior of ZnO or CuO in the composite. A previous study reported that the morphological features of the materials contribute a significant impact on the supercapacitor performance (Wei *et al*., 2021). From the inspiration from the above research results, here, we demonstrated a simple one-step facile synthesis of rGO-metal (Cu,Zn)-oxide composites as electrode materials for supercapacitors. The method is simple, inexpensive, and eco-friendly which is modified from Maity *et al*. (2018), where the utilization of hazardous chemicals such as ammonia is unfavored. The results show that the ZnO or CuO particles have more than one shape within the composite structure. Besides, their particles embedded and agglomerated over the GO surface. The effect of surface morphology, crystal structure, microstructure, and surface functional groups on the supercapacitor performance, as well as the practicality will be discussed in detail.

2. METHODS

2.1. Chemicals

The rGO was synthesized from GO, purchased from IT-Nano, Indonesia. Hexamethylenetetramine (HMT) was supplied by SCR, China. Zinc nitrate and copper nitrate were supplied by Merck Tbk, Indonesia. Deionized (DI) water was taken from Hanna Instruments SRL, Romania.

2.2. Synthesis of Reduced Graphene Oxide

Initially, 3 mg of GO powder was put into 40 mL of water and dispersed by sonication. The as-dispersed GO powder was obtained and brought into a 100-mL stainless steel autoclave and kept for 15 h at 110°C in an electrical oven. The obtained black solid precipitate was washed and collected through filtering using distilled water and ethanol. Next, the precipitate was dried for 3 h at 110°C in an oven.

2.3. Synthesis of Composites

All composites were prepared by a one-step hydrothermal method as conducted by Maity *et al*. (2018) with some modifications. To synthesize rGO-ZnO composites, 40 mL of 0.4 M zinc nitrate tetrahydrate [$Zn(NO_3)_2{\cdot}4H_2O$] solution and HMT were mixed with a 1:1 volume ratio. Then, GO powder/Zn nitrate with a mass ratio of 0.5 was added and mixed using sonication technique for 30 min. The final solution was then taken into a 100-mL stainless steel autoclave and kept for 15 h at 110°C in an oven. The obtained black with white dot precipitate was washed and collected through filtering using distilled water and ethanol. After that, it was dried for 3 h at 110 °C in an oven. rGO-CuO and rGO-ZnO-CuO composites were synthesized using a similar route to that of rGO-ZnO.

2.4. Characterizations

The properties of all composites were studied using an X-ray diffraction (XRD; Smartlab, Rigaku) with Cu Kα target (λ = 0.15404 nm), a Scanning Electron Microscope (SEM; JSM-IT200A/LA, Jeol), a Fourier Transform Infrared spectroscopy (FTIR; Nicolet iS-10 FT-IR Spectrometer, Thermo Scientific), and Raman spectroscopy (Raman iHR320, HORIBA) to identify the phase, morphology, surface functional

DOI: https://doi.org/10.17509/ijost.v8i2.56065
p- ISSN 2528-1410 e- ISSN 2527-8045

groups, and micro-structure of all composites. Raman measurement occurred at Raman shift in the range of 1000 to 2000 cm^{-1}. The composites were prepared as a twin electrode in a coin cell with KOH (1 M) as an electrolyte solution and the electrochemical properties of the composites were examined using Neware 5V 50 mA Coin Cell Tester Analyzer (TMAX Battery Equipments, China) with two electrode measurement setup.

3. RESULTS AND DISCUSSION

Figure 1 presents the XRD pattern of GO, before and after the hydrothermal process. As shown in **Figure 1a**, the GO diffractogram presents a peak at 2θ = 8.98°, which indicates a (100) plane with a hexagonal structure as the result of the formation of GO (Soltani & Lee, 2016; Sheikhzadeh *et al.*, 2018; Prabhuraj *et al.*, 2021). After the hydrothermal process, the GO peak is completely disappeared and replaced by the broad peak at 2θ = 24.61° (see **Figure 1b**), indicating the transformation of GO into rGO after the hydrothermal process at 110°C for 15 hours. The 2θ peak above 20° corresponded to the diffraction peak of rGO, as the previous report by Rai *et al.* (2021). The broad peak of rGO implies its structural defects and low crystallinity index (Wang *et al.*, 2011). Herein, most of the oxygen functional groups in the sample are removed, inducing the reduction of interlayer spacing (Park *et al.*, 2011).

The XRD pattern of rGO-(Cu,Zn)-oxide composites is shown in **Figure 2**. The peak of ZnO and ZnO_2 are identified in the XRD pattern of rGO-ZnO (see **Figure 2a**). Based on the XRD profile, the ZnO has a cubic structure. In addition, the peak identified as CuO, Cu_2O, and Cu_4O_3 is observed in the rGO-CuO XRD profile, as presented in **Figure 2b**. Whereas, the rGO-ZnO-CuO composite contains the phases which are detected in the rGO-ZnO and rGO-CuO. The peak of Zn- and Cu-hydrate are observed in all composite samples. It indicates that the rGO-(Cu,Zn)-oxide composites have some impurities, which likely come from the unreacted surfactant. The formation of Zn- and Cu-hydrate may also be related to the excessive concentration (>0.01 M) of Zn and Cu ions within the precursor solution. Alver *et al.* (2016) reported that zinc chloride hydroxide was observed when an excessive concentration of Zn ion is used during the fabrication of ZnO electrodes.

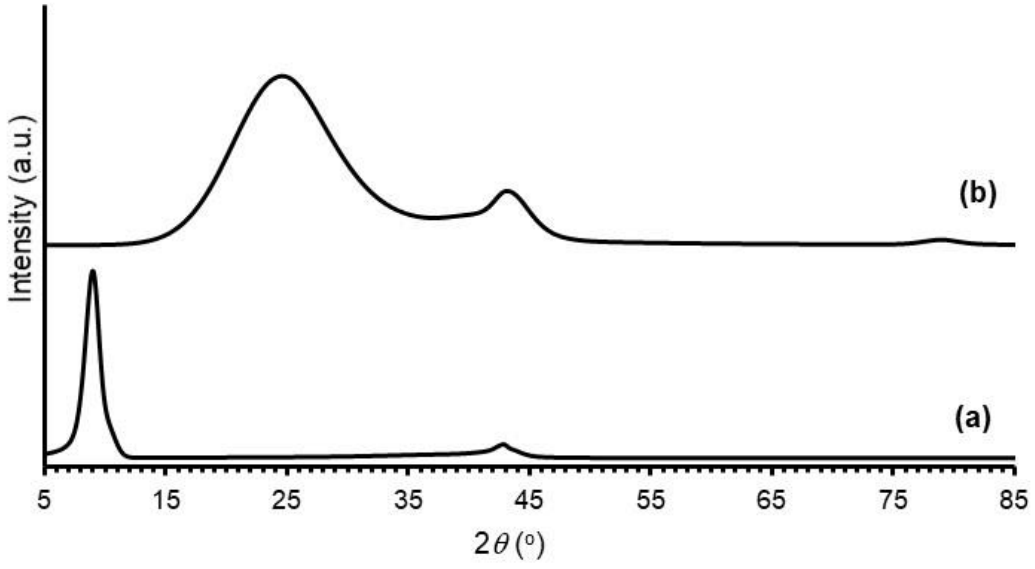

Figure 1. XRD pattern of GO: (a) before the hydrothermal process, and (b) after the hydrothermal process.

DOI: https://doi.org/10.17509/ijost.v8i2.56065
p- ISSN 2528-1410 e- ISSN 2527-8045

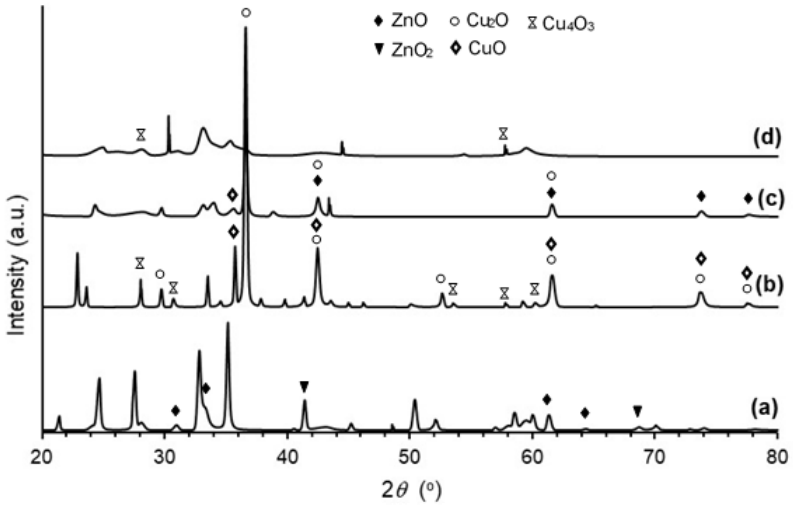

Figure 2. XRD pattern of samples: (a) rGO-ZnO, (b) rGO-CuO, (c) rGO-0.5CuO-0.5ZnO, and (d) rGO-0.25CuO-0.75ZnO.

Secondary electrons (SE) and backscattered electrons (BSE) SEM images of GO and rGO are presented in **Figures 3a-b** and **Figures 3c-d**, respectively. The morphology of GO shows a layered structure with multiple folds, which confirms that the GO in this work has a distinctive characteristic from that of previous reports (Li *et al*., 2013; Rai *et al*., 2021; Dar *et al*., 2022). **Figure 3c-d** shows that the rGO possesses abundant wrinkles and fold morphology. This is because of the existence of numerous functional groups in the GO sheet surface which disrupt the original conjugation and result in the crumpled and folded morphology with densely stacked structure after the chemical reduction (Tian *et al*., 2016). **Figure 4** presents the SEM images of the rGO-ZnO, rGO-CuO, and rGO-CuO,ZnO composites. It can be seen that all composite samples show a dark gray color with wrinkles and fold structures, which indicates the rGO characteristics as previously described in **Figure 3b**.

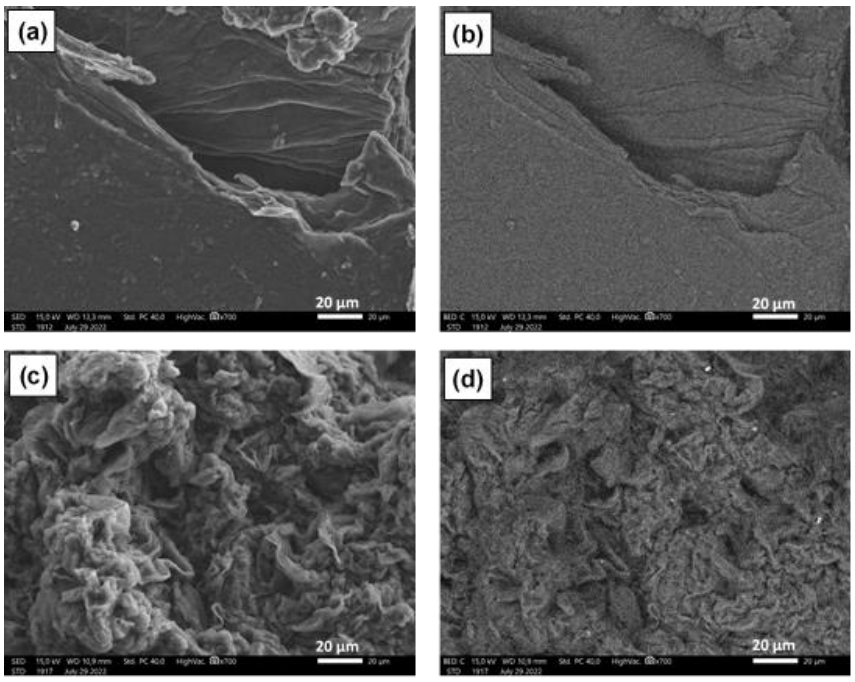

Figure 3. (a) SE SEM images of (a) GO, (b) BSE SEM image of GO, (c) SE SEM image of rGO, and (d) BSE SEM image of rGO.

DOI: https://doi.org/10.17509/ijost.v8i2.56065
p- ISSN 2528-1410 e- ISSN 2527-8045

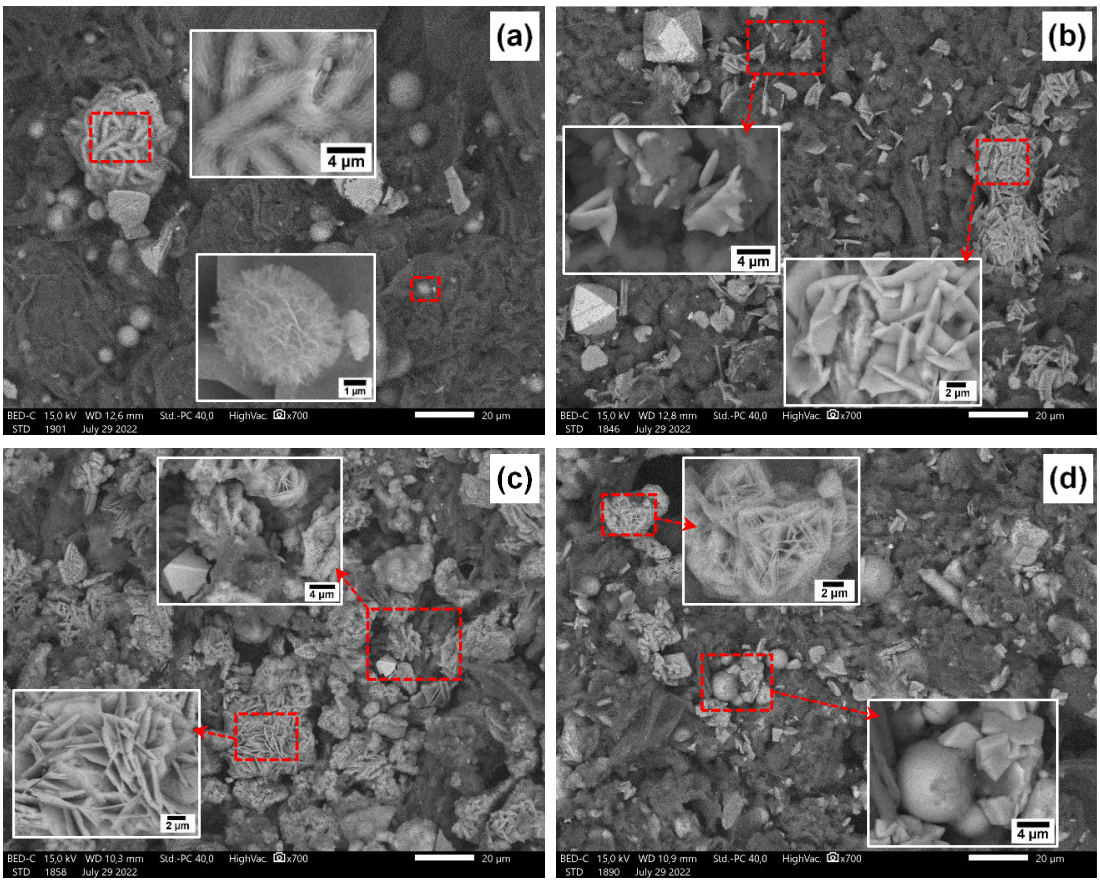

Figure 4. SEM images of the prepared samples: (a) rGO-ZnO, (b) rGO-CuO, (c) rGO-0.5CuO-0.5ZnO, and (d) rGO-0.25CuO-0.75ZnO.

It is also observed that the ZnO and CuO particles are non-homogeneously distributed on the surface and have different shapes. The ZnO and CuO particles are sandwiched in between the rGO layers. In the detailed observation using higher magnification, the ZnO particles in the rGO-ZnO (see **Figure 4a**) have fibrous shapes with nano threads, micro-spheres, as well as nanoflowers-like structures. The formation of fibrous shapes may be attributed to the relaxation of stress (Kim & Leem, 2021). These fibrous shapes appear because of insufficient time for ions to aggregate along the crystal planes which have similar lattice matches under the slow cooling after heating in the hydrothermal process. Herein, the difference in thermal expansion coefficient between the GO and ZnO should contribute to the formation of fibrous shapes during the hydrothermal process. On the other hand, the nanoflower-like-structured ZnO consists of numerous layers of nanosheets connected. The formation of nanoflower-like-structured ZnO begins with the formation of a nanosheet which is then accumulated to form the nanoflowers because of the coulomb attraction of (0001) polar surface of ZnO (Sahu & Kar, 2019), whereas ZnO spherical shape is likely formed because of the insertion of Zn ion into the gaps between sheets in the nanoflowers-like-structured ZnO during the h ydrothermal process.

The FTIR spectra of GO, rGO, rGO-ZnO, rGO-CuO, and rGO-CuO,ZnO composites are depicted in **Figure 5**. All spectra show the existence of a peak at ~ 3400 cm^{-1}, which corresponds to the COOH group (Kalaiarasi *et al*., 2021; Saranya *et al*., 2016). Apart from the GO sample, the other samples give an absorption peak at 1384 and ~ 1500 cm^{-1}, corresponding to the C–O and C=C bonding, respectively (Boukhoubza *et al*., 2020; Kalaiarasi *et al*., 2021; Saranya *et al*., 2016; Nandiyanto and Ragadhita, 2019).

DOI: https://doi.org/10.17509/ijost.v8i2.56065
p- ISSN 2528-1410 e- ISSN 2527-8045

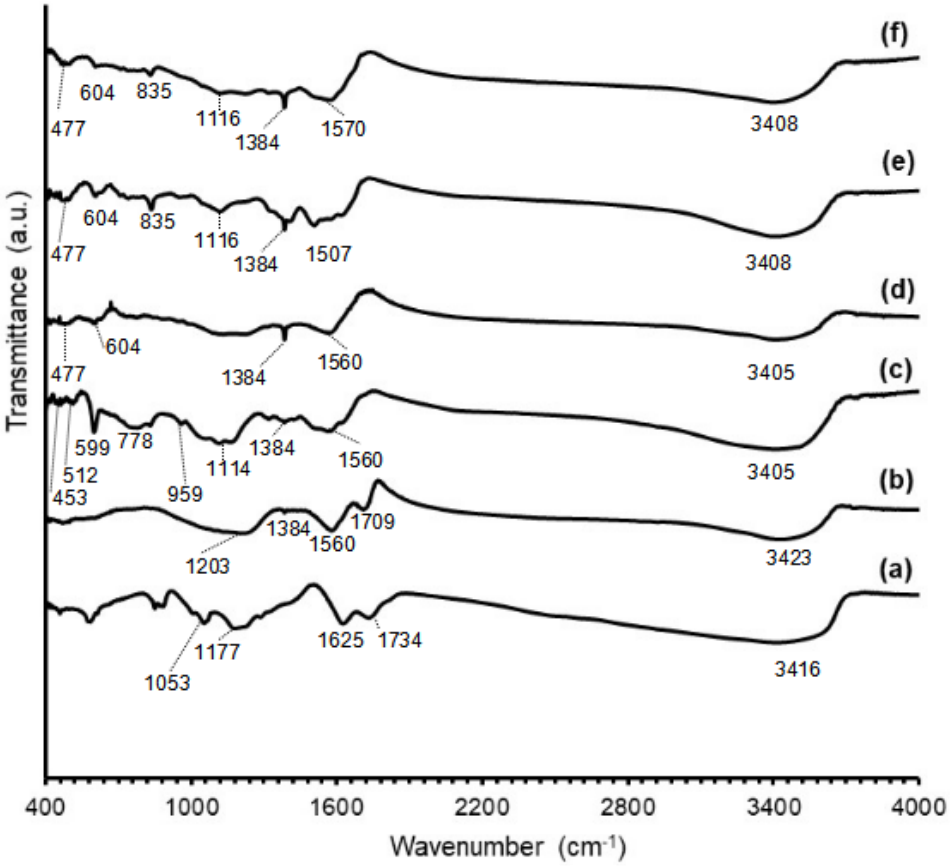

Figure 5. FT-IR Spectra of (a) GO, (b) rGO, (c) rGO-ZnO, (d) rGO-CuO, (e) rGO-0.75ZnO-0.25CuO, and (f) rGO-0.5ZnO-0.5CuO.

The GO sample gives the absorption peaks at 1053, 1177, 1625, and 1734 cm^{-1}, in which these peaks relate to the C–O bending, hydroxyl groups, C–C bond, and C=O stretching, respectively. The reduction of GO into rGO occurred after hydrothermal, indicated by the decrease of oxygen functional groups at 1057 and 1707 cm^{-1} (see **Figure 5b**) (Saranya *et al*., 2016, Rai *et al*., 2021). This also happened during the composite's synthesis as shown in **Figures 5c**–**e**. Regarding rGO-ZnO, rGO-CuO, and rGO-CuO samples, ZnO composites show the vibrational band in the range of 400 to 604 cm^{-1}, corresponding to the Zn–O, Cu–O, O–Zn–O, O–Cu–O vibration modes (Maity *et al*., 2018), indicating the formation of metal oxides. The above results are in line with the XRD and SEM characterizations in **Figure 2** and **Figure 4**, respectively. Herein, the Zn–O bond is observed at 453, 512, and 599 cm^{-1}, while the peak at 778 cm^{-1} belongs to the stretching vibration of ZnO. As shown in the previous report of Boukhoubza *et al*. (2020), the stretching vibration of ZnO is located at 812 cm^{-1}, whereas the Cu–O bond is confirmed on the absorption band of 477 and 604 cm^{-1}. A similar result was also reported by Maity *et al*. (2018).

The absorption peak at 835 cm^{-1} is obtained in the rGO-CuO,ZnO sample, which is believed as an effect of the insertion of the Cu atom into the ZnO crystal. As a result, the absorption peak at 778 cm^{-1} shifts to 835 cm^{-1}. Yet, the FTIR result undoubtedly confirmed the existence of ZnO and CuO.

Figure 6 presents the Raman spectra of GO, rGO, rGO-ZnO, rGO-CuO, and rGO-CuO,ZnO composites. All samples present the D-band and G-band around 1345 and 1599 cm^{-1}, respectively. The two characteristic bands of graphene-based material (i.e. D and G bands) correspond to the sp^3 defect or disorder and sp^2 hybridized orbitals of the C–C bond (Qin *et al*., 2014; Ramachandran *et al*., 2015; Rai *et al*., 2021; Dar *et al*., 2022).

DOI: https://doi.org/10.17509/ijost.v8i2.56065
p- ISSN 2528-1410 e- ISSN 2527-8045

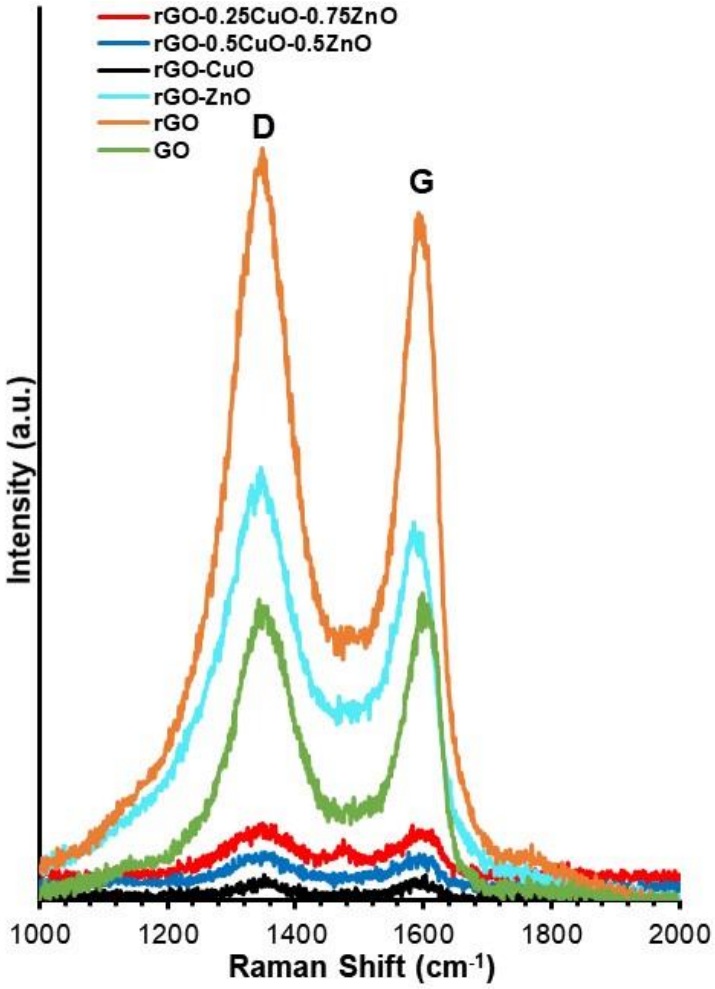

Figure 6. Raman spectra of GO, rGO, rGO-ZnO, rGO-CuO, and rGO-CuO,ZnO at Raman shift of 1000 to 2000 cm^{-1}.

The low-intensity 'D-band' and high-intensity 'G-band' (with I_D/I_G intensity ratio of 0.96) can be observed in the Raman spectra of GO, which reveals the characteristic of graphene-base material, as presented in **Figure 6a**. The results present that C–C bond is more ordered and has a small mean size of the sp^2-domain in GO materials from the synthesis of this work. Herein, the position and intensity of the D and G bands have correlation and relation to many factors, including defect, doping level, etc. Many previous reports show that the defect in graphene-based materials can be seen from the I_D/I_G intensity ratio (Ramachandran *et al.*, 2015; Rai *et al.*, 2021). The I_D/I_G intensity ratio of rGO, rGO-ZnO, rGO-CuO, and rGO-CuO,ZnO are increased (1.09, 1.18, 1.01, 1.08, and 1.12, respectively) than that of GO (0.96). As presented in **Figure 6**, the increase of I_D/I_G indicates that there is a decrease in the in-plane sp^2-domain size because of graphene-oxide reduction after the hydrothermal process, where oxygen-contained functional groups are removed.

Figure 7 presents the Raman spectra in the range of 200 to 700 cm^{-1}, giving evaluation in the vibration mode of the ZnO and CuO. It can be seen that the GO and rGO do not show a vibration peak under 700 cm^{-1}. The rGO-ZnO composite shows two major peaks at 455 and 396 cm^{-1} (**Figure 7c**). The ZnO $E_2^{(high)}$ phonon mode occurs at 455 cm^{-1}, which is because of the vibration of the O lattice (Bundesmann *et al.*, 2003; Boukhoubza *et al.*, 2020). The line at 396 has correlation to the $E_2^{(low)}$ – $E_2^{(high)}$ mode, specifically in the second-order structure of ZnO that is obtained from the transverse optical phonon (Yahia *et al.*, 2008;

DOI: https://doi.org/10.17509/ijost.v8i2.56065
p- ISSN 2528-1410 e- ISSN 2527-8045

Boukhoubza *et al*., 2020). **Figure 7d** shows the Raman spectrum of rGO-CuO, with the two major peaks at 219 and 290 cm^{-1}. The peak at 290 cm^{-1} represents the Ag mode of monoclinic CuO, originating from the vibration of the oxygen atoms (Cheng *et al*., 2021), while other peaks present in the spectrum indicate the composite peaks of rGO-CuO (Debbichi *et al*., 2012; Alajlani *et al*., 2017), the vibration peak at 219 and 290 cm^{-1} corresponded specifically to Cu_2O and CuO, respectively. The result confirms the existence of CuO and Cu_2O as Cu-oxide products after the hydrothermal process, as previously shown by the XRD analysis. The single peak is observed at 278 cm^{-1} for rGO-(0.5CuO-0.5ZnO) sample, which is similar to that of Fe-, Sb-, Al-, Ga-, and Li-doped ZnO films in a previous study (Bundesmann *et al*., 2003). In addition, Bian *et al*. (2013) also reported that the peak at 245 cm^{-1} is obtained in the Ag-doped ZnO thin films. The peak may be apart from the ZnO $E_2^{(high)}$ phonon mode at 455 cm^{-1} which appears in the edge and top backscattering configuration (Bundesmann *et al*., 2003). It may be utilized as an indication of the Cu incorporation into the ZnO lattice.

Meanwhile, rGO-(0.25CuO-0.75ZnO) composite shows a different result, where four dominant peaks (i.e. 278, 396, 455, and 535 cm^{-1}) are observed in the Raman spectrum. Previous reports showed that the peak $E_1^{(LO)}$ is approximately positioned at 584 cm^{-1} (Yahia *et al*., 2008) as well as 583 cm^{-1} (Bundesmann *et al*., 2003; Bian *et al*., 2013). Therefore, the occurrence of the peak at 535 cm^{-1} may likely be due to the formation of the defect such as an absence of oxygen, defects in the ZnO lattice resulting from the replacement of the Zn atom with Cu, and the lack of free carrier (Yahia *et al*., 2008). Current Galvanostatic charge-discharge (GCD) measurements were utilized on two cell setups in the potential range from 0 to 1 volt at a constant current density of 0.17 A/g.

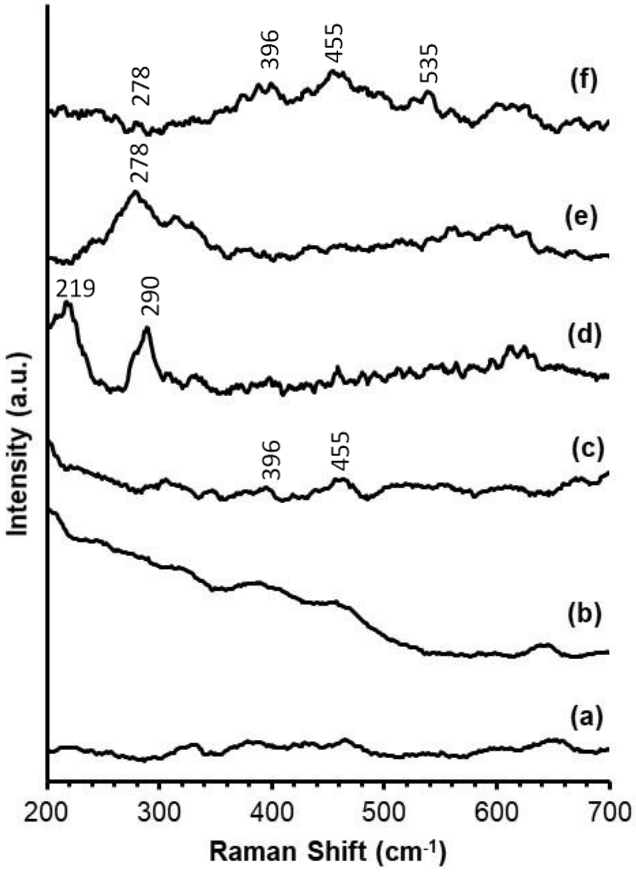

Figure 7. Raman spectra of (a) GO, (b) rGO, (c) rGO-ZnO, (d) rGO-CuO and (e) rGO-(0.5CuO-0.5ZnO) and (f) rGO-(0.5CuO-0.5ZnO).

DOI: https://doi.org/10.17509/ijost.v8i2.56065
p- ISSN 2528-1410 e- ISSN 2527-8045

Figure 8 shows the GDC analyses of rGO, rGO-ZnO, rGO-CuO, and rGO-(CuO-ZnO) composites. The GCD curves describe that the composite samples have a linear plateau as well as the pseudocapacitor and EDLC behavior (Prabhuraj *et al.*, 2018). In rGO-(CuO, ZnO, or CuO-ZnO) composites, pseudocapacitors originate from the faradic redox process of the CuO, ZnO, or CuO-ZnO. The charge storage also occurs in the form of the EDLC process due to the electrostatic interactions with rGO, where electrolytic ions get released more quickly during discharging. The results are in line with the SEM, XRD, FTIR, and Raman analysis, where the electrode contains rGO and metal (Cu-,Zn-) oxide. Besides, the symmetric nature of the charging and discharging part, indicates that the sample has an excellent super capacitive behavior (Maity *et al.*, 2018; Luo *et al.*, 2017). The specific capacitance (C_{sc}) is determined through Eq. (1) (Daragmeh, *et al*, 2017).

$$C_{sc} = \frac{2 \times I}{(\frac{dV}{dt}) \times m} \quad (1)$$

where t is the discharge time (s), I is the constant current (A), V is the potential window (V), and m is the active mass of the electrode materials (g). The calculated specific capacitance (C_{sc}) of rGO, rGO, rGO-ZnO, rGO-CuO, rGO-(0.5CuO-0.5ZnO) and rGO-(0.25CuO-0.75ZnO) composites are presented in **Table 1**. Two key factors for assessing the practical power applications of the electrochemical supercapacitor are energy density and power density. From GCD analysis, the energy density and power density of all electroactive materials can be calculated using Eq. (2) dan (3) (Maher *et al.*, 2021).

$$E = \frac{1}{2} C_{sc} \Delta V^2 \times \frac{1000}{3600} \quad (2)$$

$$P = \frac{E}{t} \times 3600 \quad (3)$$

where P is the power density (W/kg) and E is the energy density (Wh/kg). The calculation result for samples is also shown in **Table 1**. The results suggest that the specific capacitance and energy density of rGO-(CuO, ZnO, or CuO-ZnO) composites are higher than that of pristine rGO. Nevertheless, the rGO-0.5CuO-0.5ZnO composite has a smaller specific capacitance and energy density than other composites. It can be explained by the microstructure analysis, where the rGO-0.5CuO-0.5ZnO composite has a separated microstructure between the metal oxide and rGO.

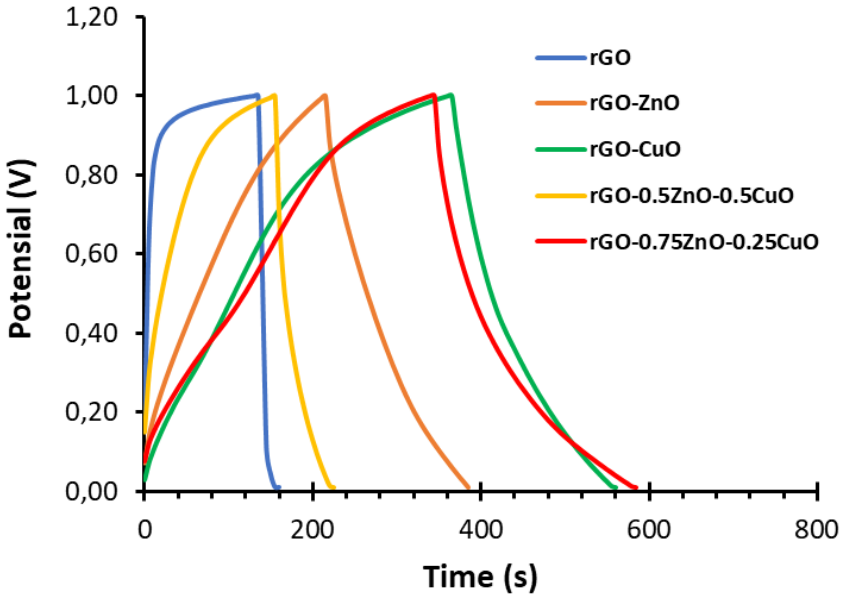

Figure 8. Comparison GCD curve of rGO, rGO-ZnO, rGO-CuO, rGO-(0.5CuO-0.5ZnO), and rGO-(0.25CuO-0.75ZnO), which measurement at a constant current density of 0.17 A/g.

DOI: https://doi.org/10.17509/ijost.v8i2.56065
p- ISSN 2528-1410 e- ISSN 2527-8045

Table 1. Specific capacitance, energy density, and power density of rGO, rGO-ZnO, rGO-CuO, and rGO-(CuO-ZnO) composites.

Materials	Specific capacitance (F/g)	Energy density (Wh/kg)	Power density (W/kg)
rGO	9.32	1.31	188.24
rGO-ZnO	58.53	8.29	175.59
rGO-CuO	54.14	7.57	143.47
rGO-(0.5CuO-0.5ZnO)	25.21	3.75	192.86
rGO-(0.25CuO-0.75ZnO)	69.27	9.93	148.92

The metal oxide experiences aggregation, forming bigger clusters with micro-flake shapes (see **Figure 4c**), which stimulates the decrease of effective contact between the electrolyte and the electrode material surface. Herein, the discharging and charging process cannot meet the optimum condition (Lo *et al*., 2020). Compared with other composites, rGO-(CuO, ZnO, or CuO-ZnO) have a structure where the CuO, ZnO, or CuO-ZnO inserts into the rGO sheet. The insertion of ZnO NRs into GO acted as electrically conductive pathways that can promote the electron transport during the charging and discharging process (Lee *et al*., 2018; Miah *et al*., 2020).

The presence of CuO, ZnO, or CuO-ZnO within the rGO structure forms the electrically conductive networks that ensure a higher rate of ion transport. Besides, the amount of mobile transport defects absorbed within the medium will affect ion mobility, which supports the charge storage capacitive behavior. A lower defect concentration obstructs ion migration within the electrolyte and increases the charge accumulation at the electrolyte-electrode interface.

These findings give information that the morphological feature of ZnO or CuO -rGO composites has a significant impact on their electrochemical properties. As reported by Wei *et al*. (2021), the abundant nanosheet and nanowires in the Co_3O_4/Ni Foam may likely contribute to the high specific capacitance, superior charge-storage feature as well as the superior electrochemical performance of the supercapacitor. In addition, the incorporation of metal-oxide (i.e. ZnO or CuO) into the rGO structure provides abundant active sites and promotes ion permeation as well as ion exchange on the rGO electrode surface. Thus, it can be considered an alternative approach to obtaining a high-performance supercapacitor.

4. CONCLUSION

The one-step hydrothermal method was successfully utilized to synthesize the rGO, rGO-ZnO, rGO-CuO, and rGO-(CuO-ZnO) composites as the electrode material for supercapacitors. The reduction of GO and direct growth of metal oxide on the rGO sheet occurred during the hydrothermal process. Apart from the metal oxide specie, XRD analysis shows the presence of other impurities after the cleaning and drying process.

Based on the SEM characterization, the Zn-oxide particles in the composite have fibrous shapes with nano threads, nanoflowers-like and micro-spheres shapes, whereas the Cu oxide particles have nanoflakes and octahedron-like shapes. The supercapacitor behavior of the composites is strongly related to their microstructure. rGO-based electrodes have a specific capacitance of 9.4 F/g, and an energy density of 1.31 Wh/kg. Whereas, rGO-ZnO, rGO-CuO, rGO-0.5CuO-0.5ZnO, and rGO-0.25CuO-0.75ZnO are found to exhibit specific capacitance and energy density of (58.53 F/g, 8.29 Wh/kg), (54.14 F/g, 7.57 Wh/kg), (25.21. F/g, 3.75 Wh/kg), and (69.27 F/g, 9.93 Wh/kg),

DOI: https://doi.org/10.17509/ijost.v8i2.56065
p- ISSN 2528-1410 e- ISSN 2527-8045

respectively. The presence of ZnO, CuO, or CuO-ZnO in the rGO-based electrode can improve the specific capacitance to some extent. In the present study, the structural modification (i.e. the insertion of CuO, ZnO, or CuO-ZnO into the rGO sheet) can significantly improve the specific capacitance and energy density of the supercapacitor.

5. ACKNOWLEDGMENT

This research was supported by DIPA-Universitas Negeri Semarang, Indonesia under Grant No. DIPA-023.17.2.677507/2022. The authors acknowledge Research Center for Advanced Materials BRIN for providing the research facilities.

6. AUTHORS' NOTE

The authors declare that there is no conflict of interest regarding the publication of this article. The authors confirmed that the paper was free of plagiarism.

7. REFERENCES

Alajlani, Y., Placido, F., Chu, H. O., Bold, R. D., Fleming, L., and Gibson, D. (2017). Characterisation of Cu_2O/CuO thin films produced by plasma-assisted DC sputtering for solar cell application. *Thin Solid Films*, *642*, 45-50.

Alver, U., Tanriverdi, A., and Akgul, O. (2016). Hydrothermal preparation of ZnO electrodes synthesized from different precursors for electrochemical supercapacitors. *Synthetic Metals, 211*, 30-34.

Aravinda L.S., Udaya Bhat K., and Ramachandra Bhat B. (2013). Nano CeO_2/activated carbon based composite electrodes for high performance supercapacitor. *Materials Letters*, *112*, 158-161.

Bian, H.Q., Ma, S.Y., Li, F.M., and Zhu, H.B. (2013). Influence of ZnO buffer layer on microstructure and raman scattering of ZnO:Ag film on Si substrate. *Superlattice and Microstructures, 58*, 171-177.

Boukhoubza, I., Khenfounch, M., Achehboune, M., Leontie, L., Carlescu, A., Doroftei, C., Mothudi, B.M., Zorkani, I., and Jorio, A. (2020). Graphene oxide coated flower-shaped ZnO nanorods: Optoelectronic properties. *Journal Alloys and Compounds*, *831*, 154874.

Bundesmann, C., Askenov, N., Schubert, M., Spemann, D., Butz, T., Kaidashev, E.M., Lorenz, M., & Grundmann, M. (2003). Raman scattering in ZnO thin films doped with Fe, Sb, Al, Ga and Li. *Applied Physics Letters*, *83*, 974-1976.

Chen, K., and Xue, D. (2014). Reaction route to the crystallization of copper oxides. *Applied Science and Convergence Technology*, *23*, 14-26.

Cheng, W., He, H., Liu, X., Liu, Y., Zhang, Z., Li, S., Zhang, R., Wang, X., Wu, Z., and Wu, Z. (2021). The study on nanostructural evolution of CuO/Graphene oxide nanocomposite during the first discharge processes. *Materials Chemistry and Physics*, *260*, 124157.

Dar, R. A., Naikoo, G. A., Srivastava, A. K., Hassan, I. U., Karna, S. P., Giri, L., Shaikh, A. M. H., Rezakazemi, M., and Ahmed, W. (2022). Performance of graphene-zinc oxide

nanocomposite coated-glassy carbon electrode in the sensitive determination of para-nitrophenol. *Scientific Reports*, *12*, 1-14.

Daraghmeh, A., Hussain, S., Saadeddin, I., servera, L., Xuriguera, E., Cornet, A., and Ciera, A. (2017). A study of carbon nanofibers and active carbon as symmetric supercapasitor in aqueous electrolyte: A comparative study. *Nanoscale Research Letters*, *12*(1), 1-10.

Debbichi, L., Marco de Lucas, M. C., Pierson, J. F., and Krüger, P. (2012). Vibrational properties of CuO and Cu_4O_3 from first-principles calculations, and raman and infrared spectroscopy. *The Journal Physical Chemistry C*, *116*, 10232-10237.

Dong S., Chen X., Zhang X., and Cui G. (2013). Nanostructured transition metal nitrides for energy storage and fuel cells. *Coordination Chemistry Reviews*, *257*(13–14), 1946-1956.

Du, X., Wang, S., Liu, Y., Lu, M., Wu, K., Lu, M. (2019). Self-assembly of free-standing hybrid film based on graphene and zinc oxide nanoflakes for high-performance supercapacitors. *Journal of Solid State Chemistry*, *277*, 441-447.

Faraji, S., and Ani, F.N. (2015). The development supercapacitor from activated carbon by electroless plating-a review. *Renewable and Sustainable Energy Reviews*, *42*, 823-834.

Firoz B. K., Siva S.S.P., Anbu K.M. 2013. Functionalisation of fabrics with conducting polymer for tuning capacitance and fabrication of supercapacitor. *Carbohydrate Polymers, 94*, 487–495.

Ghenaatian H.R., Mousavi M.F., and Rahmanifar M.S. (2012). High performance hybrid supercapacitor based on two nanostructured conducting polymers: Selfdoped polyaniline and polypyrrole nanofibers. *Electrochimica Acta*, *78*, 212-22.

Kalaiarasi, J., Pragathiswaran, C., and Subramani, P. (2021) Green chemistry approach for the functionalization of reduced graphene and ZnO as efficient supercapacitor application. *Journal of Molecular Structure*, *1242*, 130704.

Kim, D., and Leem, J.-Y. (2021). Optimal temperature of the sol–gel solution used to fabricate high-quality ZnO thin films via the dip-coating method for highly sensitive UV photodetectors. *Journal of the Korean Physical Society*, *78*, 504-509.

Kumar, H., Sharma, R., Yadav, A., and Kumari, R. (2020). Synthesis, characterization and influence of reduced Graphene Oxide (rGO) on the performance of mixed metal oxide nano-composite as optoelectronic material and corrosion inhibitor. *Chemical Data Collections*, *29*, 100527.

Lee, K.S., Park, C.W., and Kim, J.-D. (2018). Synthesis of ZnO/active carbon with high surface area for supercapacitor electrodes. *Colloids and Surfaces A*, *555*, 482-490.

Li, Z., Zhou, Z., Yun, G., Shi, K., Lv, X., and Yang, B. (2013). High-performance solid-state supercapacitors based on graphene-ZnO hybrid nanocomposites. *Nanoscale Research Letters*, *8*, 473.

Lo, A.-Y., Saravanan, L., Tseng, C.-M., Wang, F.-K., and Huang, J.-T. (2020). Effect of composition ratios on the performance of graphene/carbon nanotube/manganese oxide composites toward supercapacitor applications. *ACS Omega*, *5*, 578-587.

DOI: https://doi.org/10.17509/ijost.v8i2.56065
p- ISSN 2528-1410 e- ISSN 2527-8045

Lohar, G.M., Pore, O.C., and Fulari, A.V. (2021). Electrochemical behavior of CuO/rGO nanopellets for flexible supercapacitor, non-enzymatic glucose, and H_2O_2 sensing application. *Ceramic International*, *47*, 16674-16687.

Luo, Q., Xu, P., Qiu, Y., Cheng, Z., Chang, X., and Fan, H. (2017). Synthesis of ZnO tetratpods for high-performance supercaapcitor applications. *Materials Letters*, *198*, 192-195.

Maher, M., Hassan, S., Shoueir, K., Yousif, B., Eldin, M., and Elsoud, A. (2021). Activated carbon electrode with promising specific capacitance based on potassium bromide redox additive electrolyte for supercapasitor application. *Journal Materials Research And Technol*ogy, *11*, 1232-1244.

Maity, C. K., Hatui, G., Verma, K., Udayabhanu, G., Pathak, D.D., and Nayak, G. C. (2018). Single pot fabrication of N doped reduced GO (N-rGO)/ZnO-CuO nanocomposite as an efficient electrodematerial for supercapacitor application. *Vacuum*, *157*, 145-154.

Majeed, A., Ullah, W., Anwar, A.W., Nasreen, F., Sharif, A., Mustafa, G., and Khan, A. (2016). Graphene-metal oxide/hydroxide nanocomposite materials: Fabrication advancements and supercapacitive performance. *Journal of Alloys and Compounds, 671*, 1-10.

Miah, M., Mondal, T.K., Ghosh, A., and Saha, S.K. (2020). Study of highly porous ZnO nanospheres embedded reduced graphene oxide for high performance supercapacitor application. *Electrochimica Acta*, *354*, 136675.

Nandiyanto, A. B. D., Oktiani, R., and Ragadhita, R. (2019). How to read and interpret FTIR spectroscope of organic material. *Indonesian Journal of Science and Technology*, *4*(1), 97-118.

Otun, K.O., Xaba, M.S., Zong, S., Liu, X., Hildebrandt, D., El-Bahy, S.M., Alotaibi, M.T., El- and Bahy, Z.M. (2022). ZIF-8-derived ZnO/C decorated hydroxyl-functionalized multi-walled carbon nanotube as a new composite electrode for supercapacitor application. *Colloid and Interface Science Communiations, 47*, 100589.

Park, S., An, J., Potts, J. R., Velamakanni, A., Murali, S., and Ruoff, R. S. (2011). Hydrazine-reduction of graphite-and graphene oxide. *Carbon*, *49*, 3019-3023.

Prabhuraj, T., Prabhu, S., Dhandapani, E., Duraisamy, N., Ramesh, R., Ramesh Kumar, K.A., and Maadeswaran, P. (2021). Bifunctional ZnO sphere/r-GO composites for supercapacitor and photocatalytic activity of organic dye degradation. *Diamond and Related Materials*, *120*, 108592.

Qin, Z., Li, Z.J., Yun, G.Q., Shi, K., Li, K., and Yang, B.C. (2014). ZnO nanorods inserted graphene sheets with improved supercapacitive performance. *Applied Surface Science*, *292*, 544-550.

Rai, S., Bhujel, R., Khadka, M., Chetry, R.L., Swain, B.P., and Biswas, J. (2021). Synthesis, characterizations, and electrochemical studies of ZnO/reduced graphene oxide nanohybrids for supercapacitor application. *Materials Today Chemistry*, *20*, 100472.

Ramachandran, R., Saranya, M., Kollu, P., Raghupathy, B.P.C., Jeong, S.K., and Grace, A.N. (2015). Solvothermal synthesis of Zinc sulfide decorated Graphene (ZnS/G) nanocomposites for novel supercapacitor electrodes. *Electrochimica Acta*, *178*, 647-657.

DOI: https://doi.org/10.17509/ijost.v8i2.56065
p- ISSN 2528-1410 e- ISSN 2527-8045

Rao, M.P., Wu, J.J., Asiri, A.M., Anandan, S., and Ashokkumar, M. (2018). Photocatalytic propeties of hierarchical CuO nanosheet synthesized by a solution phase method. *Journal of Environmental Sciences*, *69*, 115-124.

Sagadevan, S., Chowdhury, Z.Z., Johan, M.R.B., Aziz, F.A., Salleh, E.M., Hawa, A., and Rafique, R.F. (2018). A one-step facile route synthesis of copper oxide/reduced graphene oxide nanocomposite for supercapacitor applications. *Journal of Experimental Nanoscience*, *13*, 284-295.

Sahu, K., and Kar, A.K. (2019). Morphological, optical, photocatalytic and electrochemical properties of hydrothermally grown ZnO nanoflowers with variation in hydrothermal temperature. *Materials Science in Semiconductor Processing*, *104*, 104648.

Saranya, M., Ramachandran, R., and Wang, F. (2016). Graphene-zinc oxide (G-ZnO) nanocomposite for electrochemical supercapacitor applications. *Journal of Science: Advanced Materials and Devices*, *1*, 454-460.

Selvakumar, M., Bhat, D.K., Aggarwal, A.M., Iyer, S.P., and Sravani, G. (2010). Nano ZnO-activated carbon composite electrodes for supercapacitors. *Physica B*, *405*, 2286-2289.

Sethi, M., Shenoy, U.S., and Bhat, D.K. (2020). A porous graphene–$NiFe_2O_4$ nanocomposite with high electrochemical performance and high cycling stability for energy storage applications. *Nanoscale Advances*, *2*, 4229-4241.

Sheikhzadeh, M., Sanjabi, S., Gorji, M., and Khabazian, S. (2018). Nano composite foam layer of CuO/graphene oxide (GO) for high performance supercapacitor. *Synthetic Metals*, *244*, 10-14.

Soltani, T., and Lee, B.K. (2017). A benign ultrasonic route to reduced graphene oxide from pristine graphite. *Journal of Colloid and Interface Science*, *486*, 337-343.

Tian, Z., Bai, S., Cao, K., and Li, J. (2016). Facile preparation of ZnO nanorods/reduced graphene oxide nanocomposites with photocatalytic property. *Materials Express*, *6*, 437-443.

Wang, H., Tian, H., Wang, X., Qiao, L., Wang, S., Wang, X., Zheng, W., and Liu, Y. (2011). Electrical conductivity of alkaline-reduced graphene oxide. *Chemical Research Chinese Universities*, *27*(5), 857-861.

Wei, G., Yan, L., Huang, H., Yan, F., Liang, X., Xu, S., Lan, Z., Zhou, W., Guo, J. (2021) The hetero-structured nanoarray construction of Co3O4 nanowires anchored on nanoflakes as a high-performance electrode for supercapacitors. *Applied Surface Science*, *538*, 147932.

Wu, F., Wang, X., Hu, S., Hao, C., Gao, H., and Zhou, S. (2017). Solid-state preparation of CuO/ZnO nanocomposites for functional supercapacitor electrodes and photocatalysts with enhanced photocatalytic properties. *International Journal of Hydrogen Energy*, *42*, 30098-30108.

Xie L.-J., Wu J.-F., Chen C.-M., Zhang C.-M., Wan L., Wang J.-L., Kong, Q.-Q., Lv, C.-X., Li, K.-X., and Sun, G.-H. (2013). A novel asymmetric supercapacitor with an activated carbon cathode and a reduced graphene oxide–cobalt oxide nanocomposite anode. *Journal of Power Sources*, *242*, 148-156.

DOI: https://doi.org/10.17509/ijost.v8i2.56065
p- ISSN 2528-1410 e- ISSN 2527-8045

Yahia, S. B., Znaidi, L., Kanaev, A., and Petitet, J.P. (2008). Raman study of oriented ZnO thin films deposited by sol-gel method. *Spectrochimica Acta Part A*, *71*, 1234-1238.

Zhou X. and Ma, L. (2015). MnO_2/ZnO porous film: Electrochemical synthesis and enhanced supercapacitor performances. *Thin Solid Films*, *597*, 44-49.

DOI: https://doi.org/10.17509/ijost.v8i2.56065
p- ISSN 2528-1410 e- ISSN 2527-8045